IEEE Access
Multidisciplinary | Rapid Review | Open Access Journal

Received October 26, 2020, accepted November 8, 2020, date of publication November 16, 2020,
date of current version November 27, 2020.

Digital Object Identifier 10.1109/ACCESS.2020.3038016

Mode Transition Control of a Power-Split Hybrid Electric Vehicle Based on Improved Extended State Observer

LONG CHEN, JIAJIA WANG, YINGFENG CAI, (Member, IEEE), DEHUA SHI, AND RUOCHEN WANG

Automotive Engineering Research Institute, Jiangsu University, Zhenjiang 212013, China

Corresponding author: Yingfeng Cai (caicaixiao0304@126.com)

This work was supported in part by the National Natural Science Foundation of China under Grant U1764257, Grant 51905219, and Grant U1664258; in part by the Natural Science Foundation of Jiangsu Province under Grant BK20190844; and in part by the Natural Science Research of Jiangsu Higher Education Institutions under Grant 19KJB580001.

ABSTRACT In order to improve the mode switching stability of a power-split hybrid electric vehicle (HEV), a torque coordinated control strategy based on disturbance observation and compensation is proposed. Aiming at the problem of engine torque disturbances caused by engine modeling error, torque control error, working environment interference and other factors, and vehicle load torque interference caused by changes in vehicle driving conditions, an improved linear extended state observer (ILESO) is designed at first. According to the deviation control principle, the state variable regulation mechanism using the same error term in the traditional linear extended state observer (TLESO) is revised, and improved by adding the corresponding deviation between the state variable and its observed value separately. Then the Lyapunov stability of the error system for the ILESO is proved gradually. On this basis, a torque redistribution algorithm of two motors based on disturbances compensation is put forward. After that, simulation verification and road adaptability analysis are carried out subsequently. The results show that the coordinated control strategy based on ILESO, compared with the TLESO, has higher observation accuracy, and makes the HEV have better vehicle speed tracking stability and mode switching smoothness when the vehicle is subject to the same external disturbance, as well as excellent adaptability under a wide range of road conditions.

INDEX TERMS Hybrid electric vehicle, mode switching, extended state observer, Lyapunov stability, disturbance compensation, adaptability.

I. INTRODUCTION

Compared with traditional vehicles, HEV has two power source systems, and could choose appropriate driving/braking modes according to different driving conditions to achieve excellent performance and power efficiency [1]–[3]. However, if the system is not controlled correctly in the mode switching process, it is easy to cause a jerk, even a significant decrease in vehicle speed, an increase in fuel consumption, and power interruption in severe cases [4]. Therefore, how to coordinate the work of multiple power sources in the mode transition process becomes the core dynamic control problem of HEV.

The associate editor coordinating the review of this manuscript and approving it for publication was Chandan Kumar.

As an essential power source of HEV, the engine itself has strong non-linearity and unpredictability, and the torque hysteresis is easily caused once the control is inaccurate, which makes the actual engine dynamic characteristics relatively complicated [5]. Instead, the AC motor usually adopts the vector control to ensure that the stator coil current is basically synchronized with the change of the output torque [6]. Based on the dynamic response gap between engine and motor, some scholars have proposed to compensate the engine response lag by adopting the method of motor torque compensation to reduce the torque fluctuation at the output shaft [7].

Huang *et al.* [8] performed a mode switching simulation test on the motor compensation control strategy of a power- split HEV, and the results showed that the drive shaft torque ripple was reduced by 53%, and no power interruption

occurred. Zhu *et al.* [9] raised a phased compensation control law based on speed tracking according to the different control stages. Ma *et al.* [10] showed that the motor control strategy based on the inertia compensation could effectively suppress the output shaft torque fluctuation of 66%. Lin *et al.* [11] also studied the effectiveness of the motor torque compensation control strategy in reducing the longitudinal jerk.

Most of the above studies only consider the hysteresis of the actual engine torque output, but ignore the fluctuation and oscillation of its resistance torque and torque output after ignition [12]. If there is no separation mechanism such as a clutch, the engine is directly connected to the wheels through the mechanical transmission parts. Therefore, the torque fluctuation interference will be transmitted to the wheels through the transmission system, affecting the driving experience of the vehicle. Chen *et al.* [13] used the motor torque to offset the torque interference problem caused by the engine start-stop switch. Wang *et al.* [14] established the transient torque fluctuation model of the engine cranking process, and applied the active damping control to reduce the jerk problem caused by engine interference. Su *et al.* [15], [16] built a transient model of the entire engine working state, and verified the effectiveness of active feedback compensation based on drive shaft torque estimation for improving the ride comfort during mode switching process. However, even though the above studies have established a more accurate engine torque fluctuation model, the model is based on the combination of cylinder pressure measurement in the engine bench test and the theoretical modeling, which inevitably ignores the interference factors such as modeling errors and actuator noise.

In addition, HEV could be easily influenced by external disturbances such as road grade changes, road adhesion coefficient changes, and sensor measurement noise under a wide range of road conditions. In severe cases, it may even deteriorate the dynamic performance of the HEV mode switching process. Sun *et al.* [17] proposed a model reference predictive control strategy, and then verified its adaptability to two roads (ordinary concrete roads and snowy roads) and different driving styles. Chiang *et al.* [18] conducted multiple stability verification tests of fuzzy sliding mode controller with different qualities and different friction coefficients. Xu *et al.* [19] demonstrated that the proposed coordinated controller has good robustness with the sinusoidal oil pressure error detection signal and the vehicle full load running at 5° gradient. It is worth noting that most of the above studies have taken the HEV mode switching response under non-interference conditions as the entry point to design a coordinated controller, which leads to relatively one-sided and low practical value research conclusions.

In summary, few studies have considered both of the above-mentioned interference at the same time, but both the engine torque fluctuation interference and the driving condition interference do have a serious impact on the mode switching quality of HEV. Therefore, it is of great practical significance to explore the dynamic coordination controllers that have excellent anti-interference ability against the above-mentioned two kinds of interference.

At present, the commonly used anti-interference methods include active disturbance rejection control [20], adaptive control [21], robust control [22], adaptive robust control [23] and so on. Sun *et al.* [24] proposed an adaptive control method that can effectively solve the parameter uncertainty and external interference of the pneumatic artificial muscle system. Pan and Sun [25] designed a disturbance estimator to estimate the unmeasurable state variables and disturbances in the active suspension control of vehicles, and realized the anti-jamming performance of the suspension through feedback compensation control. Yang *et al.* [26] put forward a feedback control method for tower crane based on nonlinear observer. Most of the anti-interference methods mentioned above accurately estimate the system interference by designing an observer, and then achieve the effect of interference suppression through appropriate compensation control, thereby achieving excellent robust stability of the entire closed-loop system. The extended state observer (ESO) [27] is a commonly used tool for estimating interference and parameter uncertainty. Yao and Deng [28] designed a TLESO with a maximum observer gain of 42875, which makes it relatively sensitive to noise, and is prone to slow convergence and low accuracy. Pu *et al.* [29] proposed a fixed-time convergent fal function and three new nonlinear ESO structures. However, the algorithm of this observer is complicated, which greatly increases the arduousness of data processing in the control unit.

Based on this, from the design perspective of an anti-interference coordinated controller, a power-split hybrid electric vehicle with double-planetary gears is taken as the research object. The main contributions and innovations of this paper are threefold: (a)the essence of the E-H mode switching jerk is deeply revealed, and the effectiveness of basic motor torque compensation control strategy for improving the mode switching quality is also clarified; (b)taking into account the fluctuation characteristics of engine transient torque and the variability of vehicle driving conditions, a coordinated control algorithm for interference suppression based on state observer estimation and compensation is proposed; (c)Aiming at the large observation error of the high-gain TLESO, an ILESO is further designed. Finally, the estimation accuracy of ILESO and the effectiveness and adaptability of the feedback compensation coordinated control strategy based on ILESO are verified by simulation test.

The outline of this paper is organized as follows. In Section II, the transient driveline model of the power-split HEV is built. In Section III, the mode transition process is divided into three stages, and the basic motor torque compensation control is presented. Then the problem statement is illustrated in Section IV, and the coordinated control strategy based on ILESO is proposed in Section V. The corresponding simulation results are given in Section VI. Finally, Section VII gives the conclusion.

II. MODELLING OF THE POWER SPLIT SYSTEM WITH DOUBLE-PLANETARY GEARS

A. THE POWER SPLIT SYSTEM WITH DOUBLE-PLANETARY GEARS

The power-split system studied in this paper is shown in Figure 1. Wherein, the engine is connected to the planet carriers of the front PG, the motor MG1 is connected to the sun gear of the front PG, while the motor MG2 is connected to the sun gear of the rear PG. The ring gear of the rear PG is fixed. The front gear ring and the rear planet carrier are connected together to transmit and then output power. In particular, the decoupling of the engine speed and torque could be achieved by controlling MG1 and MG2. Meanwhile, the engine speed could be regulated by adjusting the torque of MG1, thereby changing the operating range of the engine and reducing the fuel consumption.

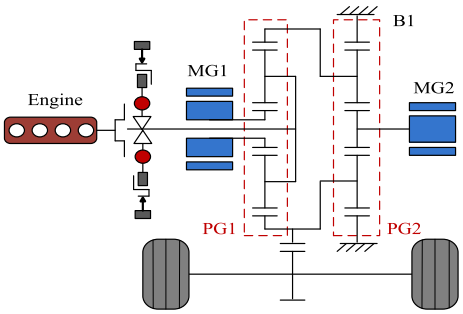

FIGURE 1. The power-split system with double-Planetary gears.

According to the working state of the power sources and the brake, eight working modes of this power-split HEV could be realized: MG2 single driving mode, MG1 and MG2 combined driving mode, engine independent driving mode, hybrid driving mode, parking charging mode, composite braking mode, mechanical braking mode and parking mode. Among them, the typical working modes are shown in Table 1. Since the E-H switching process from the electric driving mode to the hybrid driving mode involves various intermediate states such as the starting and speed regulating process of the engine, it is more complicated than the other switching process. Therefore, this paper focuses on the dynamic characteristics of the system during the E-H switching process.

TABLE 1. Typical working modes.

Working modes	Engine	MG1	MG2	B1	Description
Electric driving mode	Off	On	On	Lock	Low speed and load, large SOC
Hybrid driving mode	On	On	On	Lock	Increased vehicle load, low SOC

B. THE TRANSIENT MODEL CONSTRUCTION

1) ENGINE AND MOTOR MODEL

In consideration of the time delay of engine, this paper uses the combination of "engine steady-state lookup table model" and "first-order inertial delay module" to characterize the dynamic properties of the engine [30]:

$$T_E = \frac{1}{\tau_E s + 1} f(\omega_E, \alpha) \tag{1}$$

Among them, T_E and ω_E are the output torque and speed of the engine, respectively. τ_E is the time constant of the engine torque response, and f is the mapping function between the steady-state torque of the engine, the throttle opening α, and the engine speed, which is usually constructed from engine bench test data.

Similar to the engine, the dynamic models of MG1 and MG2 also use a combination of experimental modeling and theoretical modeling to establish a quasi-steady-state look-up table model. Take MG2 as an example:

$$T_{MG2} = \frac{1}{\tau_m s + 1} T_{MG2-o} \tag{2}$$

Among them, T_{MG2} is the output torque of the motor MG2, τ_m is the time constant of the motor torque response, and T_{MG2-O} is the target torque of the motor.

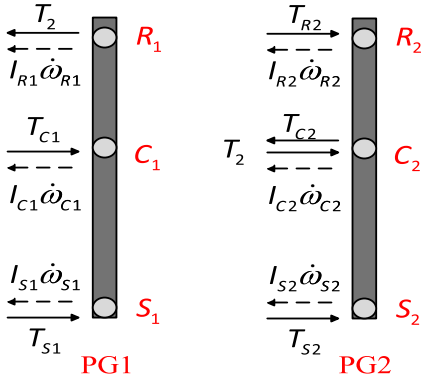

FIGURE 2. The lever diagram.

2) POWER COUPLING MECHANISM MODEL

To realistically simulate the dynamic performances of a power-split HEV, it is necessary to build the transient model. Ignoring the inertia of the planet gears, the elasticity and damping of the system, the lever model of the double-planetary gears shown in Figure 2 can be obtained. Among them, I_{R1}, I_{C1} and I_{S1} are the concentrated inertia of the ring gear, the carrier and the sun gear in the front PG1, respectively. w_{R1}, w_{C1} and w_{S1} are the angular velocity of the members mentioned above, respectively. The same goes for the rear planetary gears. T_2 is the internal torque between the front ring and rear carrier, T_{R2} is the external torque acting on the ring gear R2, and T_{C2} is the external torque from the vehicle at the output shaft end of the coupling device, while

T_{C1}, T_{S1} and T_{S2} represent the external torque of the engine, MG1 and MG2 respectively.

According to the leverage model, the following equation of the front PG1 can be obtained:

$$\begin{cases} T_{S1} + T_{C1} - T_2 = I_{R1}\dot{\omega}_{R1} + I_{C1}\dot{\omega}_{C1} + I_{S1}\dot{\omega}_{S1} \\ T_{S1}(1+k_1) + T_{C1} = I_{C1}\dot{\omega}_{C1} + I_{S1}\dot{\omega}_{S1}(1+k_1) \end{cases} \tag{3}$$

Similarly, the torque balance equation of PG2 is as follows:

$$\begin{cases} T_{S2} - T_{C2} + T_2 + T_{R2} = I_{R2}\dot{\omega}_{R2} + I_{C2}\dot{\omega}_{C2} + I_{S2}\dot{\omega}_{S2} \\ T_{S2}k_2 - T_{R2} = -I_{R2}\dot{\omega}_{R2} + I_{S2}\dot{\omega}_{S2}k_2 \end{cases} \tag{4}$$

where,

$$T_{S1} = T_{MG1} - I_{MG1}\dot{\omega}_{MG1} \tag{5}$$
$$T_{S2} = T_{MG2} - I_{MG2}\dot{\omega}_{MG2} \tag{6}$$
$$T_{C1} = T_E - I_E\dot{\omega}_E \tag{7}$$
$$T_{C2} = T_{out} + I_{out}\dot{\omega}_{out} \tag{8}$$
$$T_{out} = T_{req} + T_{brk} \tag{9}$$

where T_{MG1}, I_{MG1} and w_{MG1} are the output torque, inertia and rotational speed of motor MG1, respectively. T_{MG2}, I_{MG2} and w_{MG2} are the output torque, inertia and rotational speed of motor MG2, respectively. T_E, I_E and w_E are the output torque, inertia and rotational speed of the engine, respectively. T_{out} represents the output load, including the equivalent resistance torque T_{req} of the vehicle running resistance and the equivalent resistance torque T_{brk} of the braking torque. I_{out} is the equivalent inertia of the vehicle mass, and w_{out} is the output speed of the carrier C2. k_1 and k_2 represent the characteristic parameters of the front and rear planetary gears, respectively.

According to the connection method and the unique speed relationship of the planetary gears, it can be known that:

$$\omega_{S1} + k_1\omega_{R1} = (1+k_1)\omega_{C1} \tag{10}$$
$$\omega_{S2} + k_2\omega_{R2} = (1+k_2)\omega_{C2} \tag{11}$$
$$\omega_{R1} = \omega_{C2} = \omega_{out} \tag{12}$$
$$\omega_{S1} = \omega_{MG1} \tag{13}$$
$$\omega_{S2} = \omega_{MG2} \tag{14}$$
$$\omega_{C1} = \omega_E \tag{15}$$
$$\omega_{R2} = 0 \tag{16}$$

Then it can be obtained that:

$$\begin{bmatrix} T_E + (1+k_1)T_{MG1} \\ T_E + T_{MG1} + (1+k_2)T_{MG2} - T_{out} \end{bmatrix} = \begin{bmatrix} I_{11} & I_{12} \\ I_{21} & I_{22} \end{bmatrix} \begin{bmatrix} \dot{\omega}_E \\ \dot{\omega}_{out} \end{bmatrix} \tag{17}$$

where

$$I_{11} = I_E + I_{C1} + (1+k_1)(I_{MG1} + I_{S1}) \tag{18}$$
$$I_{12} = I_{out} + I_{R1} + I_{C2} - k_1(I_{MG1} + I_{S1}) + (I_{MG2} + I_{S2})(1+k_1)^2 \tag{19}$$
$$I_{21} = I_E + I_{C1} + (I_{MG1} + I_{S1})(1+k_1)^2 \tag{20}$$
$$I_{22} = -k_1(1+k_1)(I_{MG1} + I_{S1}) \tag{21}$$

III. BASIC MOTOR TORQUE COMPENSATION CONTROL(BMTCC) DURING E-H MODE TRANSITION PROCESS

The E-H mode transition process consists of three phases: pure electric phase, engine cranking phase and hybrid driving phase. Fig.3 gives a corresponding staged BMTCC diagram. Among them, according to the energy management strategy that has been set in advance [31], the vehicle required torque T_{req} is allocated to each power source, and the corresponding steady-state target torque T_{E-EMS}, $T_{MG1-EMS}$, $T_{MG2-EMS}$ are derived, so as to achieve the optimal fuel economy of the vehicle. Then taking into account the tasks of each stage, the BMTCC is given for the purpose of reducing the mode switching jerk. More details could be found below.

When the hybrid vehicle is operating in the pure electric driving mode, the engine torque is 0, and the motor MG1 controls the engine at the zero speed point as shown in fig.3(a). The output speed and torque of the power coupling device remain unchanged. At this time, the whole vehicle works in the steady-state pure electric mode, so that the torque distribution of the energy management strategy is the target torque output of BMTCC, namely T_{E-0}, T_{MG1-0} and T_{MG2-0}. The target torques of two motors are as follows:

$$T_{MG1-0} = k_{p1}(\omega_E - 0) + k_{i1}\int(\omega_E - 0)dt \tag{22}$$
$$T_{MG2-0} = \frac{1}{1+k_2}T_{req} \tag{23}$$

Among them, k_{p1} and k_{i1} are the proportional and integral parameters in the MG1 controller to regulate the engine speed, respectively. The common empirical method is adopted to achieve the parameter adjustment.

When the vehicle speed exceeds a certain threshold V_{thr} (this paper is set to 32km/h), the pure electric mode can not meet the driving demand. It is necessary to start the engine to idle speed (900r/min) within 0.5s [32], and make the longitudinal jerk lower than the German limit standard (10m/s^3). Considering the fast response characteristics of the motor, the MG2 torque could be used to compensate the torque ripple caused by engine start. As shown in fig.3(b), the extra torques in BMTCC module to start the engine and to reduce the jerk are added to MG1 and MG2 separately. Thus the target torques of two motors are as follows:

$$T_{MG1-0} = -\frac{1}{1+k_1}T_{ef} + \frac{I_{21}}{1+k_1}\dot{\omega}_{E-t\,\mathrm{arg}\,et} \tag{24}$$
$$T_{MG2-0} = \frac{1}{1+k_2}T_{req} - \frac{k_1}{(1+k_1)(1+k_2)}T_{ef} + \Delta T_{MG2-0} \tag{25}$$
$$\Delta T_{MG2-0} = (\frac{I_{11}}{1+k_2} - \frac{I_{21}}{(1+k_1)(1+k_2)})\dot{\omega}_E \tag{26}$$

where T_{ef} is the starting resistance torque of the engine. During the engine cold start process, the temperature of the cylinder and the piston are relatively low, the resistance torque increases with the rise of the engine speed, and the initial increase rate is slow. When the idle speed is about to be

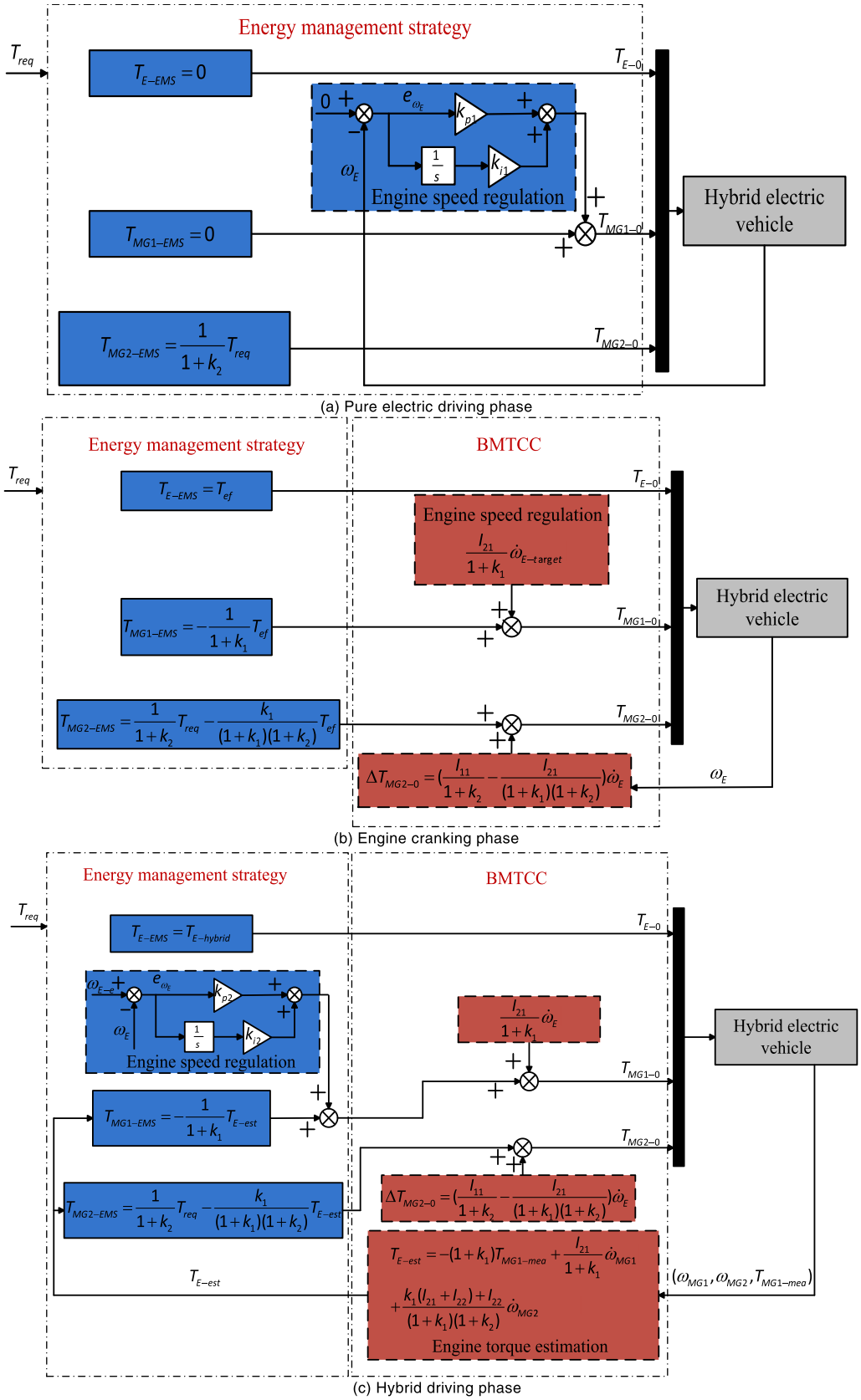

FIGURE 3. The BMTCC diagram.

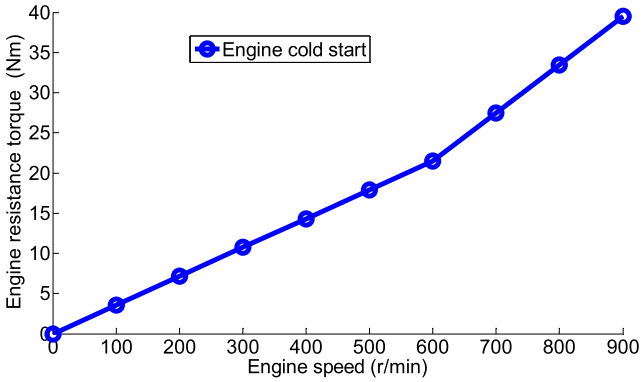

FIGURE 4. Engine cold start resistance torque.

reached, the resistance torque rises rapidly. Finally, the relationship between the resistance torque and the rotational speed is shown in Figure 4 [33].

Once the engine speed exceeds the idle speed, the power-split HEV quickly switches to the hybrid driving mode. At this time, the engine outputs torque and drives the vehicle together with MG2. Then MG1 regulates the engine to work at the economic speed (1500r/min). Considering the lag characteristics of the engine torque and the unique structural properties of the planetary gear, the actual engine torque is estimated in real-time using two motor dynamics during the engine speed regulation phase:

$$T_{E-est} = -(1+k_1)T_{MG1-mea} + \frac{I_{21}}{1+k_1}\dot{\omega}_{MG1} + \frac{k_1(I_{21}+I_{22})+I_{22}}{(1+k_1)(1+k_2)}\dot{\omega}_{MG2} \quad (27)$$

As shown in Figure 3(c), BMTCC includes the jerk compensation module of MG1, jerk compensation module of MG2 and engine torque estimation module. Thereby the comprehensive compensation control law of MG1 and MG2 are obtained:

$$T_{MG1-0} = -\frac{1}{1+k_1}T_{E-est} + \frac{I_{21}}{1+k_1}\dot{\omega}_E + \Delta T_{MG1-0} \quad (28)$$

$$\Delta T_{MG1-0} = k_{p2}(\omega_{E-e} - \omega_E) + k_{i2}\int(\omega_{E-e} - \omega_E)dt \quad (29)$$

$$T_{MG2-0} = \frac{1}{1+k_2}T_{req} - \frac{k_1}{(1+k_1)(1+k_2)}T_{E-est} + \Delta T_{MG2-0} \quad (30)$$

In order to reveal the mechanism of jerk more intuitively, the basic motor torque coordination strategy is simulated and analyzed by Matlab/Simulink software. The dynamic response characteristics of the system as shown in Fig. 5 can be obtained. The critical components of the whole vehicle are shown in Table 2.

As can be seen from Fig. 5, the vehicle works in the purely electric mode (mode 1) in the initial stage. At this time, the motor MG2 separately output torque to drive the car and

TABLE 2. Key Component Parameters of HEV.

Parameters		Value
Engine	Maximum power(speed)	54kW(4700r/min)
	Maximum torque	115Nm
MG1	Maximum power(speed)	15kW(8000r/min)
	Maximum torque	55Nm
MG2	Maximum power(speed)	30kW(12000r/min)
	Maximum torque	305Nm
Battery	capacity	6.5Ah
	Rated voltage	288V
Characteristic parameters of PG	The front PG1	1.842
	The rear PG2	2.48
Vehicle	Mass (full load) m	1398kg
	Frontal area A	1.746m^2
	Air resistance coefficient C_D	0.3
	Rolling drag coefficient f_{roll}	0.01
	Rolling radius R_t	0.287m
	Main reducer speed ratio i_o	3.93
	K_{p1}/k_{i1}	0.025/0.015
	K_{p2}/k_{i2}	0.5/0.0001

made it better to track the ideal vehicle speed, and there is no obvious longitudinal jerk of the vehicle.

When the vehicle speed reaches 32km/h at 10.67s, the vehicle controller sends a mode switching signal, then MG1 towing the engine from a static condition to its idle state, which causes an obvious jerk in the negative direction. During the engine cranking phase, the torque change rate of MG1 increases rapidly, while the torque change rate of MG2 is low, but the engine resistance torque is negatively increasing. The vehicle's driving resistance torque remains unchanged, thus it causes a negative jerk at this stage. Simultaneously, MG2 adjusts its torque to drive the vehicle to continue tracking the target vehicle speed, but the tracking effect is deteriorated.

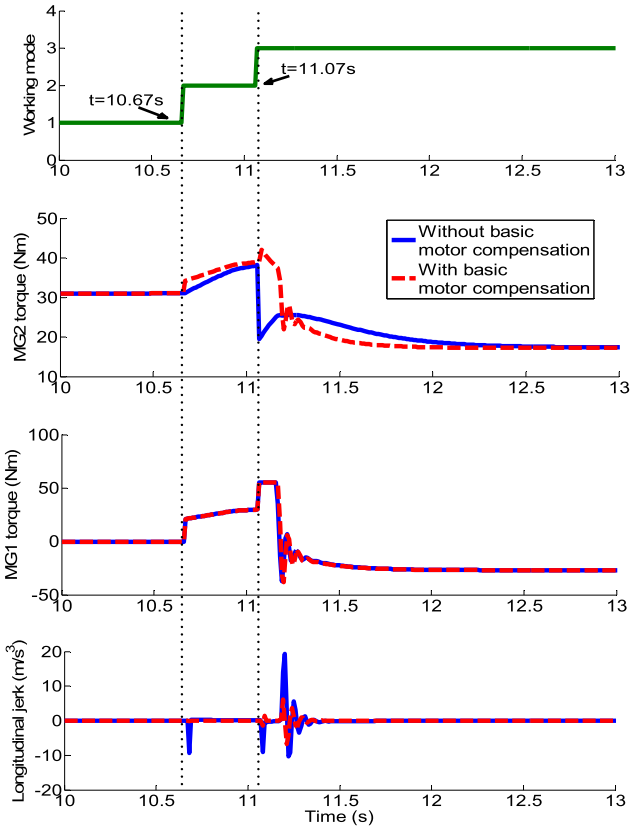

FIGURE 5. System responses during the E-H mode transition process.

When the engine speed reaches its idle speed at 11.07s, it starts to inject fuels and ignite. Then the vehicle enters into the hybrid driving mode (mode 3). However, due to the formulation of the energy management strategy, the power split HEV must go through an engine speed regulation stage before it can enter a stable hybrid driving mode. During this regulation stage, the vehicle produces a large positive and negative jerk. The negative jerk at this stage is mainly caused by the output torque of MG1, while the positive jerk is mainly due to the engine output torque. Until the engine is stable at the economic operating point, the vehicle works in a stable hybrid driving mode, and the E-H mode switching process ends. In a word, when the BMTCC is adopted, the MG2 torque is increased timely during the engine cranking phase, and moderately decreased in the initial stage of the hybrid driving mode, thereby significantly reducing the longitudinal jerk.

IV. PROBLEM STATEMENT

The effectiveness of the above-mentioned BMTCC strategy is based on the assumption that the torque executions of the power sources are accurate, the entire closed-loop control system is time-invariant, and there is no parameter uncertainty and external interference. However, in the actual driving process, hybrid electric vehicles are susceptible to interference from engine, road grade changes, rolling resistance coefficient, actuator noise, and sensor measurement noise [34].

Engine is the main source of system fluctuations and response delay [35]. Regardless of the simplified "steady-state Map + first-order inertia module" model or the complex engine average model, the modeling errors are unavoidable. At the same time, due to the non-linearity, uncertainty and environment influence, accurate engine torque control is also difficult to achieve [36].

In addition, Chen and Sun [37] showed that the main disturbance factors affecting the mode switching response during HEV mode switching include not only the engine torque execution interference, but also the load torque interference. Due to the variability of road conditions, HEV is directly affected by road interference, which in turn causes chain changes in load torque. It is the road surface interference that directly acts on the vehicle, resulting in a significant longitudinal jerk.

Therefore, the design of a dynamic coordinated control strategy for hybrid electric vehicles that considers the above interference has important practical significance for real vehicle applications.

V. THE COORDINATED CONTROL STRATEGY BASED ON ILESO

Based on this, various disturbance factors such as engine modeling error and actuator error are integrated into engine torque interference d_1. The disturbances such as the road slope and the rolling resistance coefficient are unified and integrated into the output load disturbance as d_2.

Because of the importance of engine dynamic performance and road conditions for mode switching smoothness, this paper focuses on these two disturbances. From equation (17), the coupling mechanism model including the disturbances could be obtained:

$$\begin{bmatrix} \dot{\omega}_E \\ \dot{\omega}_{out} \end{bmatrix} = B \cdot \begin{bmatrix} T_E + d_1 + T_{MG1} + (1+k_2)T_{MG2} - T_{out} - d_2 \\ T_E + d_1 + (1+k_1)T_{MG1} \end{bmatrix} \tag{31}$$

$$B = \begin{bmatrix} I_{11} & I_{12} \\ I_{21} & I_{22} \end{bmatrix}^{-1} \tag{32}$$

Then it could be transformed into the following state-space model:

$$\dot{x}_1 = B \cdot U + d \tag{33}$$

$$x_1 = \begin{bmatrix} \omega_E \\ \omega_{out} \end{bmatrix} \tag{34}$$

$$U = \begin{bmatrix} T_E + T_{MG1} + (1+k_2)T_{MG2} - T_{out} \\ T_E + (1+k_1)T_{MG1} \end{bmatrix} \tag{35}$$

$$d = B \cdot \begin{bmatrix} d_1 - d_2 \\ d_1 \end{bmatrix} \tag{36}$$

According to the principle of the extended observer, a new extended state vector is constructed:

$$\bar{X} = d \tag{37}$$

Then the TLESO of the system is:

$$e_1 = z_1 - x_1 \tag{38}$$

$$\dot{z}_1 = z_2 + B \cdot U - \beta_0 e_1 \tag{39}$$
$$\dot{z}_2 = -\beta_1 e_1 \tag{40}$$

Among them, z_1 and z_2 are the real-time estimated value of the state vector x_1 and the extended state vector $\bar{X}$, respectively. Where

$$\beta_0 = \begin{bmatrix} \beta_{01} & 0 \\ 0 & \beta_{02} \end{bmatrix} \tag{41}$$
$$\beta_1 = \begin{bmatrix} \beta_{11} & 0 \\ 0 & \beta_{12} \end{bmatrix} \tag{42}$$

$\beta_{01}, \beta_{02}, \beta_{11}, \beta_{12}$ are all positive numbers.

It can be seen from the Eq.39-40 that the tracking adjustment of z_1 and z_2 both need to be achieved by controlling the error e_1, so that they could track the target value respectively. But for the extended state observer, making z_1 fast track on x_1 is the primary target, followed by z_2 approaching d. Once this sequence is out of order, the system adjustment will fail. Obviously, the system controls z_1 and z_2 at the same time. Under this mechanism, when z_1 has not stably tracked x_1, it is of little significance to control z_2 to approach d. When z_1 stable tracking x_1 is completed, the adjustment of z_2 becomes relatively difficult because e_1 is already very small. In order to achieve the effective adjustment of z_2, the TLESO is only made by selecting a larger gain β_1, but an excessive gain will reduce the dynamic performance of the observer. Therefore, it is not appropriate to adjust the derivative of z_2 with the error e_1 according to the deviation control principle, and it is necessary to find a suitable deviation to replace e_1.

It could be deduced from the formula (38-39):

$$\begin{cases} z_1 = e_1 + x_1 \\ z_2 = \dot{z}_1 - B \cdot U + \beta_0 e_1 \end{cases} \tag{43}$$

Further

$$z_2 = x_2 + \dot{e}_1 + \beta_0 e_1 \tag{44}$$

It can be seen that the error between z_2 and x_2 is $\dot{e}_1 + \beta_0 e_1$, and the rapid convergence of the system could be speed up by adding it as a control variable. Based on this idea, an ILESO is constructed:

$$\begin{aligned} e_1 &= z_1 - x_1 \\ \dot{z}_1 &= z_2 + B \cdot U - \beta_0 e_1 \\ \dot{z}_2 &= -\beta_1 \left[\dot{e}_1 + (\beta_0 + 1) e_1\right] \end{aligned} \tag{45}$$

If

$$\begin{aligned} X_1 &= e_1 = z_1 - x_1 \\ e_2 &= z_2 - d \end{aligned} \tag{46}$$

Then

$$\begin{aligned} \dot{X}_1 &= \dot{e}_1 = X_2 \\ &= \dot{z}_1 - \dot{x}_1 = z_2 + B \cdot U - \beta_0 e_1 - B \cdot U - d \\ &= e_2 - \beta_0 e_1 \end{aligned} \tag{47}$$

In that way, the system equation of the observation error is:

$$\begin{aligned} \dot{X}_1 &= X_2 \\ \dot{X}_2 &= \dot{e}_2 - \beta_0 \dot{e}_1 = \dot{z}_2 - \dot{d} - \beta_0 X_2 \\ &= -(\beta_1 + \beta_0) X_2 - w - \beta_1 (\beta_0 + 1) X_1 \end{aligned} \tag{48}$$

According to the Barbashin formula, the Lyapunov function is attempted to be found:

$$V = \frac{\beta_0 \beta_1 (\beta_0 + 1) X_1^2 + \beta_0 X_2^2}{\beta_0 + \beta_1} \tag{49}$$

Then its derivative is:

$$\dot{V} = \frac{\partial V}{\partial X_1} \dot{X}_1 + \frac{\partial V}{\partial X_2} \dot{X}_2 = -2\beta_0 X_2^2 - 2\frac{\beta_0}{\beta_0 + \beta_1} X_2 w(t) \tag{50}$$

where

$$\dot{d} = w(t) \tag{51}$$

It can be obtained that V is positive definite and has infinite properties from the condition that β_0 and β_1 are positive values. When $w(t) = 0$, the following conclusion could be summarized:

$$\dot{V} < 0 \tag{52}$$

Therefore, the zero point of the error system is globally asymptotically stable. When the disturbance $w(t)$ is not equal to 0, and the maximum absolute value is w_0, there will be a certain error in the observed value. That is:

$$\begin{aligned} |e_1| &\le \frac{w_0}{\beta_1 (\beta_0 + 1)} \\ |e_2| &\le \frac{\beta_0 w_0}{\beta_1 (\beta_0 + 1)} \end{aligned} \tag{53}$$

Similarly, according to the formula (46-48) in the above text to define the observation error system of TLESO. After the system reaches the steady state, the following formula is satisfied:

$$\dot{X}_1 = 0, \dot{X}_2 = 0 \tag{54}$$

Then the steady state error range of TLESO could be obtained:

$$\begin{aligned} |e_1| &\le \frac{w_0}{\beta_1} \\ |e_2| &\le \frac{\beta_0 w_0}{\beta_1} \end{aligned} \tag{55}$$

Compared with eq.(53), the observation error of ILESO is $1/(\beta_0+1)$ of the TLESO, and the observation accuracy is greatly improved.

By designing the ILESO shown in eq. (45), the estimated value of the comprehensive interference Z_2 can be obtained, then the estimated values of engine torque disturbance d_1 and load disturbance d_2 are further calculated as follows:

$$\begin{bmatrix} \hat{d}_2 \\ \hat{d}_1 \end{bmatrix} = \begin{bmatrix} I_{21} - I_{11} & I_{22} - I_{12} \\ I_{21} & I_{22} \end{bmatrix} Z_2 \tag{56}$$

In summary, the mode switching control block diagram of HEV shown in Fig.6 is proposed. Among them, the driver

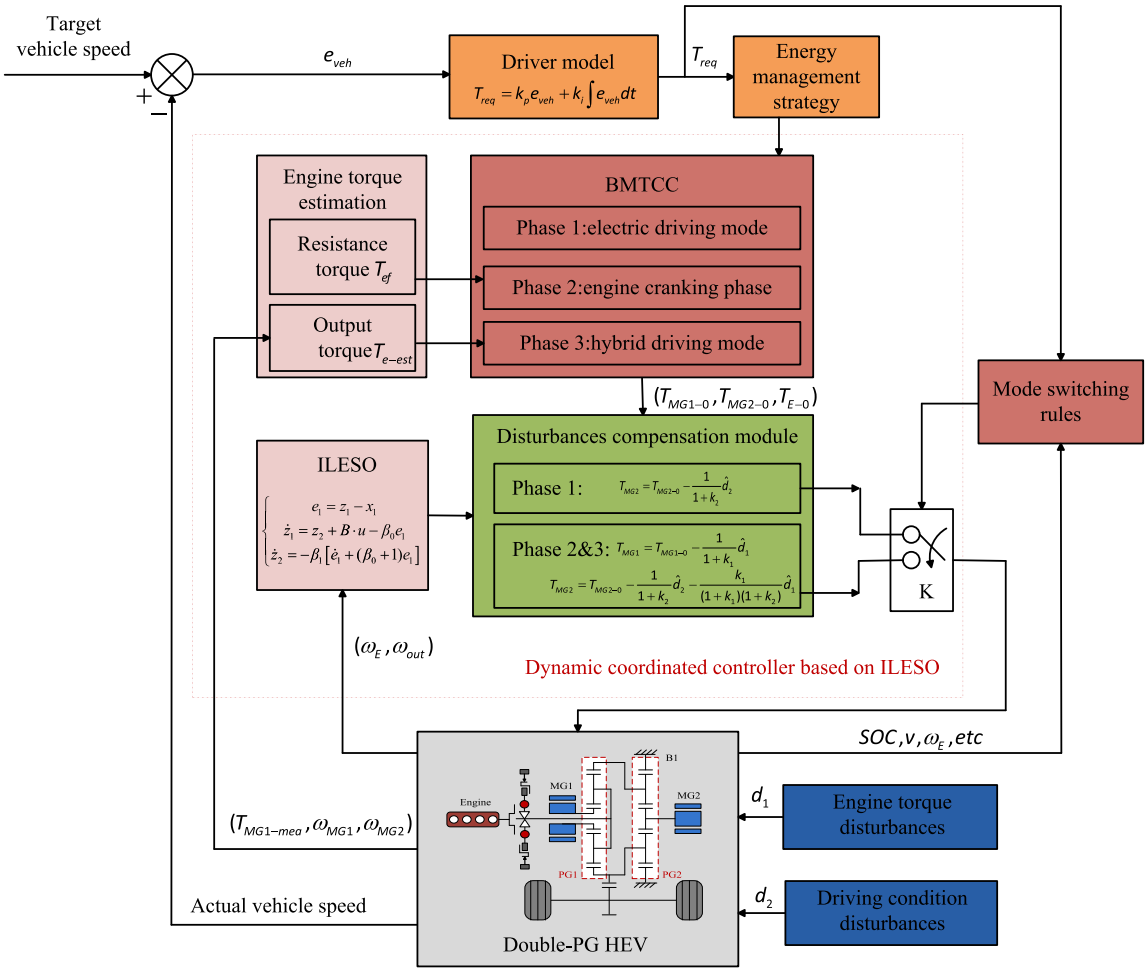

FIGURE 6. Block diagram of mode switching control for hybrid electric vehicle.

model is simulated by PI control, and the difference between the target vehicle speed and the actual speed is taken as the input. By adjusting the proportional and the integral coefficient, the vehicle demand driving torque T_{req} can be calculated to ensure the vehicle speed tracking. The BMTCC strategy then decouples the T_{req} to the initial target torque T_{E-0} of the engine, T_{MG1-0} of MG1 and T_{MG2-0} of MG2. According to the three stages of the E-H mode switching process, the expressions of the initial target torque of each power sources shown in eq. (22-30) are derived.

Since the mode switching process is susceptible to interference from engine torque and driving conditions, an ILESO is designed for real-time estimation. By collecting the actual engine speed ω_E and output shaft speed ω_{out} signals, the deviation between each state variable and its observed value is used as the adjustment basis for the state variable, thereby outputting the interference estimation value to the disturbance compensation module. According to the current driving information of the HEV, such as SOC, vehicle speed, and other signals and the established mode switching rules, the sub-switching controller K matches the interference compensation control in different switching stages at appropriate time. Thus, the dynamic coordination controller of the entire HEV is formed, including the BMTCC module, the engine torque estimation module, the ILESO module and the disturbances compensation module. The multiple Lyapunov method is adopted to design the Lyapunov functions for the three subsystems of mode switching, which can verify the global asymptotic stability of the coordinated controller. In particular, the following torque compensation redistribution strategy at each stage in the disturbances compensation module could reduce the impact of external interference:

1) Electric driving phase

$$T_{MG2} = T_{MG2-0} - \frac{1}{1+k_2}\hat{d}_2 \tag{57}$$

2) Engine cranking phase and hybrid driving phase

$$T_{MG1} = T_{MG1-0} - \frac{1}{1+k_1}\hat{d}_1 \tag{58}$$

$$T_{MG2} = T_{MG2-0} - \frac{1}{1+k_2}\hat{d}_2 - \frac{k_1}{(1+k_1)(1+k_2)}\hat{d}_1 \tag{59}$$

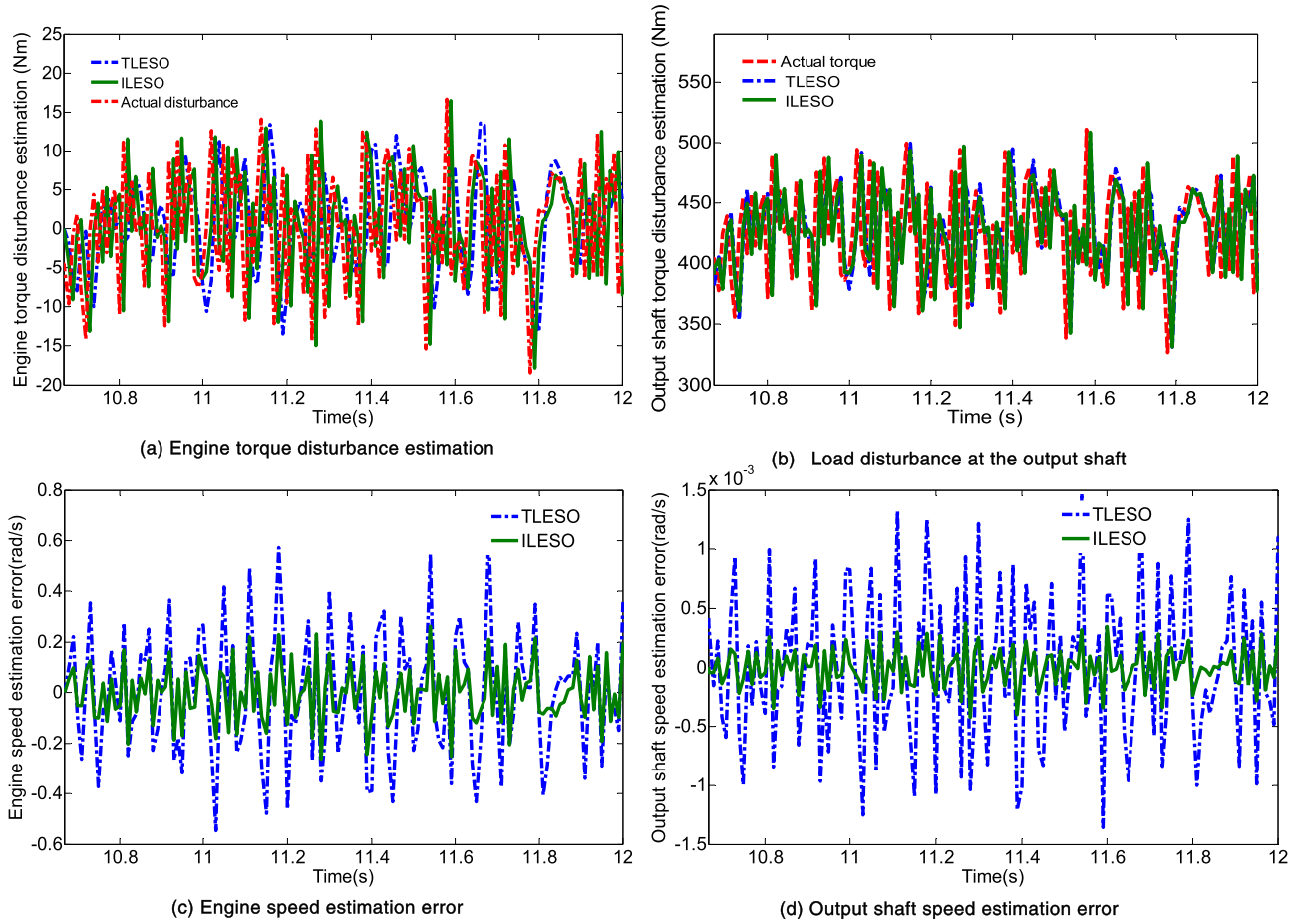

FIGURE 7. Estimation error comparison between TLESO and ILESO.

VI. SIMULATION ANALYSIS

A. EFFECTIVENESS OF THE ILESO

In order to verify the effectiveness of the proposed coordinated control strategy, Gaussian white noise with a bandwidth of 20 Hz and a variance of 20 Nm and 100 Nm are used to simulate the engine torque output disturbance d_1 and the output load disturbance d_2 [9], [37]. At the same time, a simulation form of adding noise separately is adopted to reveal the influence of the two kinds of interference on the mode switching response in depth. Among them, the observation gain matrices in ILESO in this paper are $\beta_0 = diag\{50\ 100\}$, $\beta_1 = diag\{50110\}$. The specific parameter adjustment method of the observer is as follows: First, according to the Hurwitz stability criterion of the observer error system, the gain range that makes the system stable is obtained; Then the desired disturbance observation bandwidth of the observer is set referring to the dynamic characteristics of the disturbance, and the final gain value is determined according to the pole configuration method.

Fig.7 shows the estimation comparison of the two extended state observers. Obviously, there are apparent deviations at multiple time points of TLESO for engine disturbance and load disturbance, while the estimation of ILESO is more accurate. Meanwhile, the steady-state observation errors of ILESO for the state variables ω_E and ω_{out} are also smaller than that of TLESO, and the observation error could be reduced by 1 to 2 orders of magnitude. Therefore, compared with the traditional linear/non-linear ESO, the ILESO proposed in this paper can not only reduce the complexity of the algorithm, but also improve the observation accuracy, which lays the foundation for the subsequent application of the proposed coordinated control strategy for interference compensation.

B. EFFECTIVENESS OF THE COORDINATED CONTROL BASED ON ILESO

It can be seen from Fig. 8(d-e) that when the HEV does not adopt any interference compensation coordinated control strategy, the engine torque interference obviously deteriorates the smoothness of stage 2 and stage 3 and the stability of the vehicle speed tracking. Moreover, this kind of interference has not been noticed by the upper controller, and the torque commands of the motors MG1 and MG2 are still issued by the pre-set basic coordinated controller (green dotted line in Fig. 8 (b-c)). However, the disturbances compensation coordinated control strategy based on ILESO could quickly

TABLE 3. Comparison of coordinated control effects based on two observers.

Disturbance type	Observer type	RMS value of interference estimation error	Maximum longitudinal jerk (m/s^3)	Maximum error of vehicle speed tracking (m/s)
Engine torque disturbance d_1	TLESO	3.43	9.80	0.0331
	ILESO	1.67	8.21	0.0328
Load disturbance d_2	TLESO	14.95	10.46	0.0339
	ILESO	5.82	9.74	0.0338

and accurately estimate the current interference signal value (Fig. 8(a)). Subsequently, the torques of the motor MG1 and MG2 are re-determined through the interference compensation strategy shown in eq. (57-59) (Fig.8 (b-c) red line). Finally, the longitudinal jerk of the hybrid driving mode is significantly reduced, and the stability of vehicle speed tracking is improved either(Fig.8(d-e)). Compared with the strategy without interference compensation, the coordinated control strategy based on TLESO can also improve the mode switching quality, but due to the inability to accurately estimate the engine torque interference, the corresponding jerk and speed tracking error are obviously worse than the coordinated control strategy based on ILESO.

Fig.9 shows the comparison of the three coordinated control effects when the hybrid vehicle is disturbed by the load at the output shaft. It can be seen from Fig.9(d-e) that the load disturbance greatly deteriorates the quality of the entire mode switching, causing a positive impact with a peak value of 24.5m/s^3, and the vehicle speed tracking error oscillation is obvious. However, the coordinated control based on ILESO finally controls the longitudinal jerk of the vehicle within [-10m/s^3, 10m/s^3], and realizes a relatively stable vehicle speed tracking at the same time by accurately estimating the load interference (Fig.9(a)) and the torque re-compensation of MG2 (Fig.9(c)). In addition, since the observation error of the two observers on the torque disturbance at the output shaft is small, the mode switching quality of the coordinated control strategy based on ILESO is slightly better than that of the strategy based on TLESO.

Based on Fig. 8-9, it can be seen that, compared to the engine torque disturbance, the equivalent load interference at the output caused by changes in vehicle driving conditions has a greater impact on the hybrid vehicle's mode switching response and is more difficult to be eliminated. Table 3 shows the comparison of the coordinated control based on TLESO and ILESO. It can be seen from the table that ILESO, compared with TLESO, has higher estimation accuracy, and its coordinated controller has better suppression of the longitudinal jerk during the mode switching process, and the corresponding vehicle speed tracking is also more stable. Simultaneously, the estimation accuracy of the observer has an obvious positive correlation with the smoothness of mode switching and target vehicle speed tracking.

In summary, the coordinated control strategy based on ILESO designed in this paper could significantly improve the mode switching smoothness and vehicle speed tracking stability, and even exhibit a certain degree of anti-interference ability.

C. ADAPTABILITY OF THE ILESO-BASED COORDINATED CONTROL TO A WIDE RANGE OF ROAD CONDITIONS

Generally speaking, the roads for vehicles mainly include asphalt/concrete roads, gravel roads, dirt roads and icy roads on rainy and snowy days, and the corresponding rolling resistance coefficient is in the range of [0.01,0.03]. Similarly, according to China's highway route design specifications, the maximum longitudinal slope of the highway plain hilly area is 3%, and the maximum slope of the first-class automobile highway plain hilly area is 4%, so the general road slope should be [0,4%] [38].

Based on this, the random distributions of the above parameter intervals are used to simulate the random change of the road conditions in a wide range (Fig.10(a), Fig. 11(a)). And the corresponding load torque change is obtained by the vehicle running resistance torque formula shown in eq. (60), as shown in Fig.10(b) and 11(b).

$$T_{out} = R_t \cdot [mgi + mgf_{roll} + \frac{1}{2}\rho C_D A v^2 + ma] \quad (60)$$

where i is the road gradient, v is the longitudinal vehicle speed, and a is the acceleration.

The random road conditions shown in Figs. 10(a) and 11(a) are added separately to the vehicle simulation model to obtain the coordinated control effect diagrams shown in Fig. 10-11(c-d). As shown in Fig.10, when the rolling resistance coefficient changes randomly, the mode switching jerk and vehicle speed tracking error both increase significantly, even up to 16.4m/s^3 and 0.068m/s, respectively.

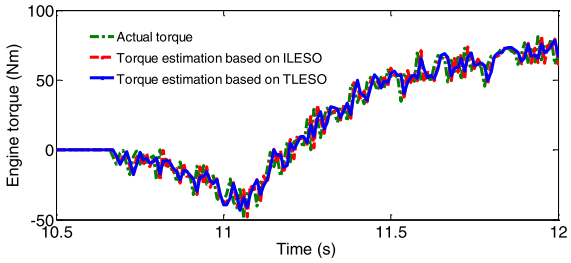

(a) Engine torque estimation

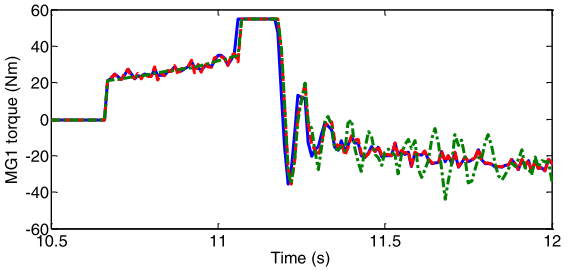

(b) MG1 torque

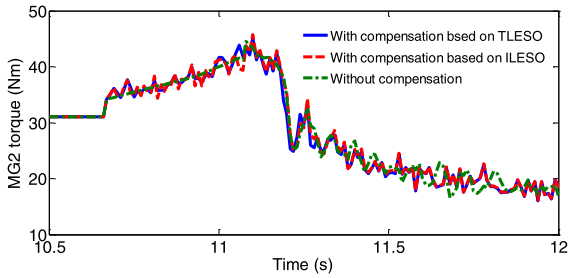

(c) MG2 torque

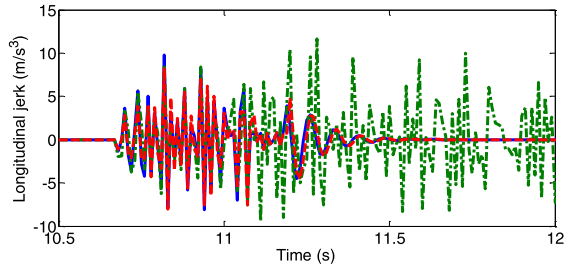

(d) Longitudinal jerk

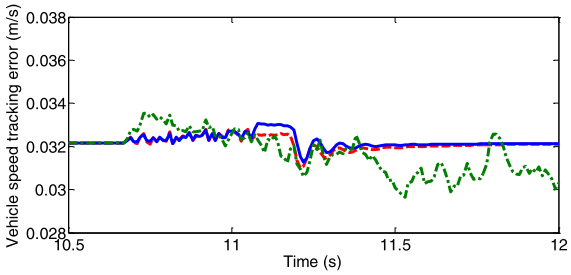

(e) Vehicle speed tracking error

FIGURE 8. **Comparison of three kinds of coordinated control effects under the engine torque disturbance.**

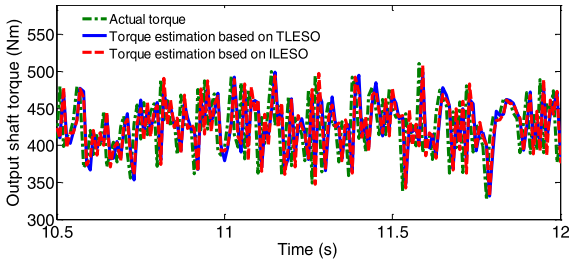

(a)Load disturbance estimation at the output shaft

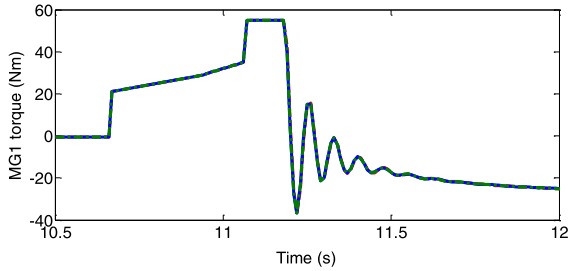

(b) MG1 torque

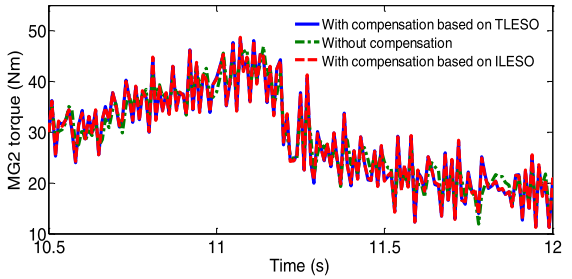

(c) MG2 torque

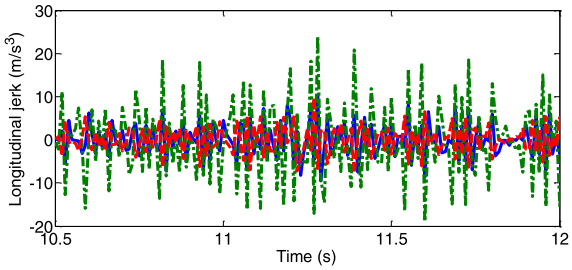

(d) Longitudinal jerk

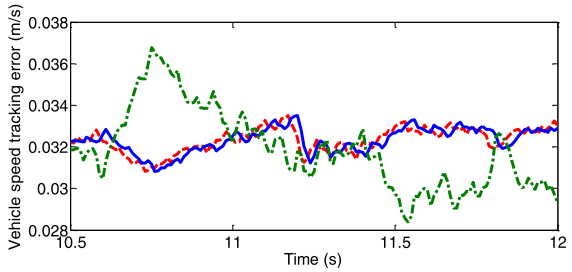

(e) Vehicle speed tracking error

FIGURE 9. **Comparison of three kinds of coordinated control effects under the load disturbance at the output shaft.**

However, the coordinated control strategy based on ILESO could effectively control the jerk within [-4.6m/s^3,5.4m/s^3], and also significantly reduce the speed tracking error by estimating the interference. Similarly, Fig.11(c-d) also depicts the effectiveness of the coordinated control strategy when the road gradient changes randomly from two aspects of the mode switching comfort and vehicle speed tracking effect.

According to fig.10-11, it can be concluded that when the coordinated control strategy of interference compensation is not adopted, HEV is more sensitive to road gradient changes than the road rolling resistance coefficient. This is mainly

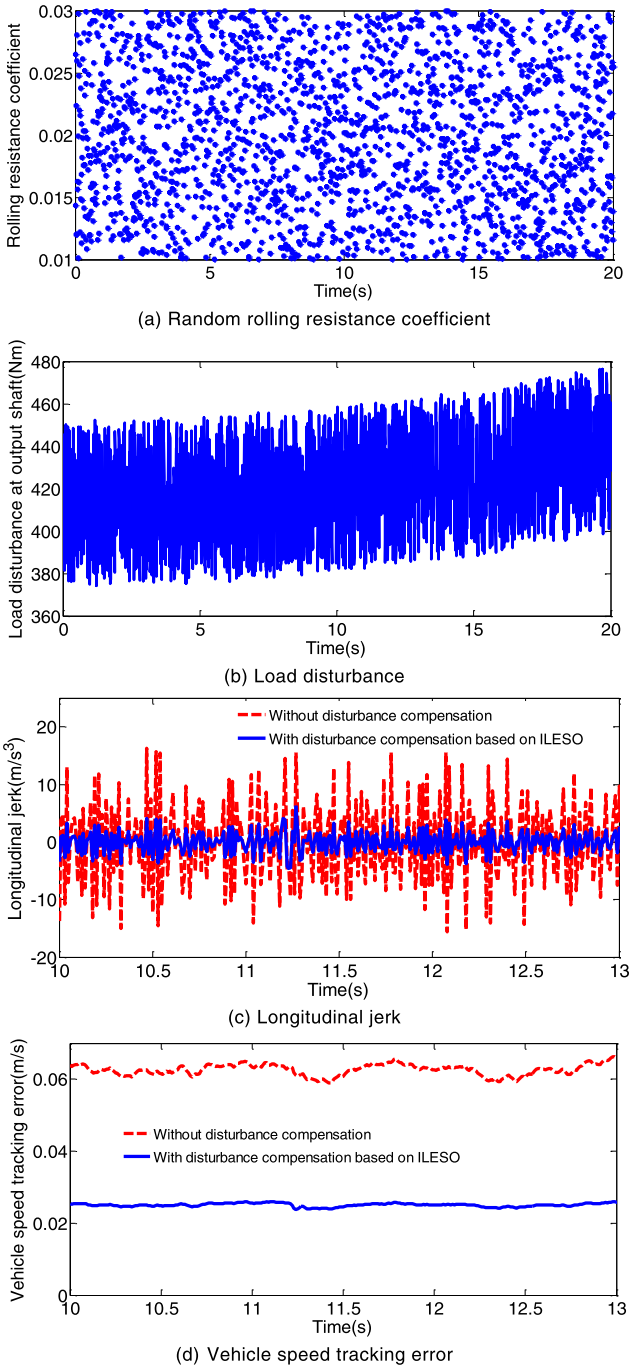

FIGURE 10. Coordinated control effect when rolling resistance coefficient is random.

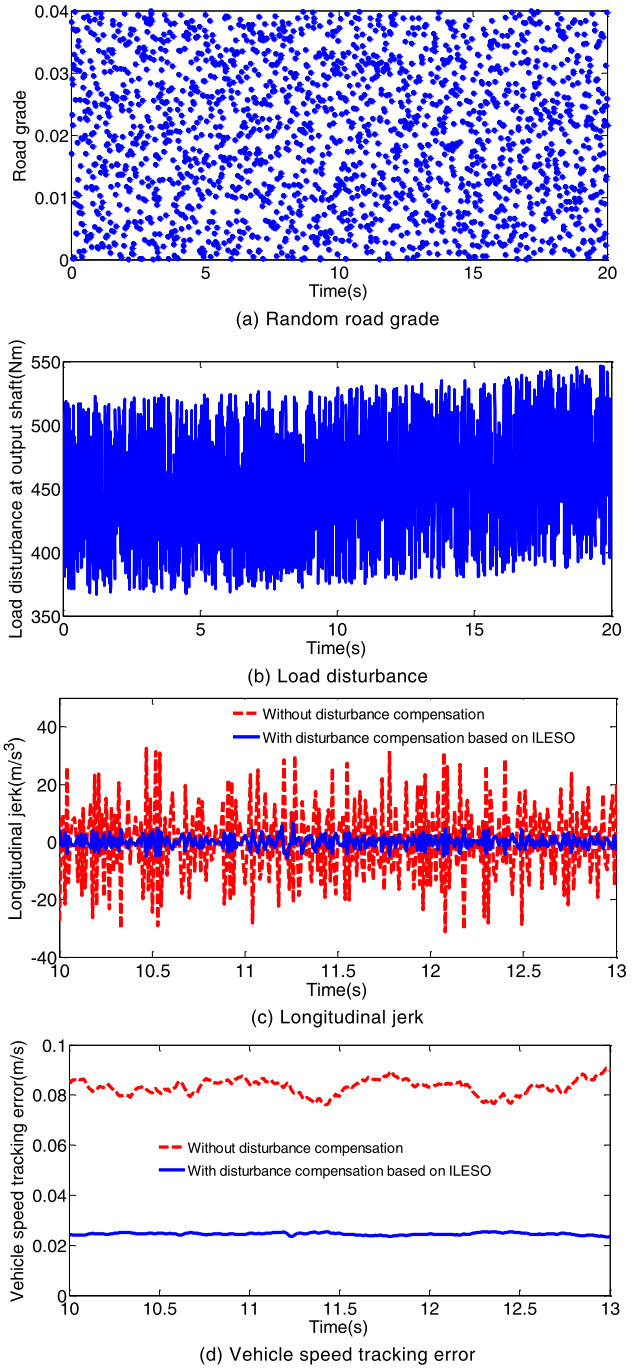

FIGURE 11. Coordinated control effect when road grade is random.

because the corresponding driving resistance changes are more severe, which causes higher jerk and vehicle speed tracking errors. After adopting the coordinated control strategy based on ILESO, whether it is the change of the road rolling resistance coefficient or the road slope, HEV has good adaptability to both, and the corresponding control effect is similar. In summary, the ILESO-based coordinated control strategy proposed in this paper has excellent adaptability and important practical application value for a wide range of road conditions.

VII. CONCLUSIONS

By studying the dynamic characteristics of the E-H mode switching process for the power-split hybrid electric vehicle, the corresponding transient vehicle model is built, and the jerk caused by engine lag is analyzed, and the typical basic motor torque compensation coordinated control strategy is further introduced.

Taking into account the disturbance characteristics of the engine torque and variable driving conditions, a coordinated control strategy composed of an improved linear extended

state observer and a torque redistribution module with system disturbances compensation is proposed. Then through the Matlab/Simulink simulation platform, the anti-interference of the strategy, the smoothness of the mode switching quality and the adaptability to a wide range of road conditions are finally verified.

Subsequent research will comprehensively consider disturbance factors such as system time delay and parameter perturbation, and seek a robust coordinated controller with excellent anti-interference ability, which has certain guiding significance and reference value for the future engineering practice.

REFERENCES

[1] J. Zhang, T. Shen, and J. Kako, "Short-term optimal energy management of power-split hybrid electric vehicles under velocity tracking control," *IEEE Trans. Veh. Technol.*, vol. 69, no. 1, pp. 182–193, Jan. 2020.

[2] X. Zeng and J. Wang, "A parallel hybrid electric vehicle energy management strategy using stochastic model predictive control with road grade preview," *IEEE Trans. Control Syst. Technol.*, vol. 23, no. 6, pp. 2416–2423, Nov. 2015.

[3] S. Xie, H. He, and J. Peng, "An energy management strategy based on stochastic model predictive control for plug-in hybrid electric buses," *Appl. Energy*, vol. 196, pp. 279–288, Jun. 2017.

[4] A. Gao, Z. Fu, and F. Tao, "Dynamic coordinated control based on sliding mode controller during mode switching with ICE starting for an HEV," *IEEE Access*, vol. 8, pp. 60428–60443, Mar. 2020.

[5] B. X. Wen, W. D. Wang, C. L. Xiang, and Y. L. Zhao, "Torque coordinated control for the multi-power in parallel-series HEV," *J. Harbin Inst. Technol*, vol. 48, no. 1, pp. 72–79, Jan. 2016.

[6] Y. Tong, "Study on the coordinated control issue in parallel hybrid electric system," Ph.D. dissertation, Dept. Power Eng., Tsinghua Univ., Beijing, China, 2004.

[7] J. Wang, Y. Cai, L. Chen, D. Shi, R. Wang, and Z. Zhu, "Review on multi-power sources dynamic coordinated control of hybrid electric vehicle during driving mode transition process," *Int. J. Energy Res.*, vol. 44, no. 8, pp. 6128–6148, Jun. 2020.

[8] K. Huang, C. L. Xiang, Y. Ma, W. D. Wang, and R. Langari, "Mode shift control for a hybrid heavy-duty vehicle with power-split transmission," *Energies*, vol. 10, no. 2, pp. 1–18, Feb. 2017.

[9] F. Zhu, L. Chen, C. Yin, and J. Shu, "Dynamic modelling and systematic control during the mode transition for a multi-mode hybrid electric vehicle," *Proc. Inst. Mech. Engineers, D, J. Automobile Eng.*, vol. 227, no. 7, pp. 1007–1023, Jul. 2013.

[10] Y. Ma, K. Huang, C. Xiang, W. Wang, and H. Liu, "A control strategy to reduce torque variation for dual-mode power-split hybrid electric vechile during mode shift," in *Proc. 7th Int. Conf. Model., Identificat. Control (ICMIC)*, Dec. 2015, pp. 1–8.

[11] Y. P. Lin, D. T. Qin, Y. G. Liu, and Y. Yang, "Control strategy for all the mode-switches of hybrid electric vehicle," *Adv. Mech. Eng*, vol. 8, no. 11, pp. 1–17, Nov. 2016.

[12] D. H. Liu, "Dynamics study of a power-split hybrid electric vehicle during the engine start transition," Ph.D. dissertation, Dept. Mech. Eng., Shanghai Jiao Tong Univ., Shanghai, China, 2017.

[13] J.-S. Chen and H.-Y. Hwang, "Engine automatic start–stop dynamic analysis and vibration reduction for a two-mode hybrid vehicle," *Proc. Inst. Mech. Engineers, D, J. Automobile Eng.*, vol. 227, no. 9, pp. 1303–1312, Sep. 2013.

[14] C. Wang, Z. Zhao, T. Zhang, and M. Li, "Mode transition coordinated control for a compound power-split hybrid car," *Mech. Syst. Signal Process.*, vol. 87, pp. 192–205, Mar. 2017.

[15] Y. Su, M. Hu, L. Su, D. Qin, T. Zhang, and C. Fu, "Dynamic coordinated control during mode transition process for a compound power-split hybrid electric vehicle," *Mech. Syst. Signal Process.*, vol. 107, pp. 221–240, Jul. 2018.

[16] Y. Su, L. Su, M. Hu, D. Qin, C. Fu, and H. Yu, "Modeling and dynamic response analysis of a compound power-split hybrid electric vehicle during the engine starting process," *IEEE Access*, vol. 8, pp. 186585–186598, 2020.

[17] J. Sun, G. Xing, X. Liu, X. Fu, and C. Zhang, "A novel torque coordination control strategy of a single-shaft parallel hybrid electric vehicle based on model predictive control," *Math. Problems Eng.*, vol. 2015, pp. 1–12, Jun. 2015.

[18] C. J. Chiang, Y. C. Chen, and C. Y. Lin, "Fuzzy sliding mode control for smooth mode changes of a parallel hybrid electric vehicle," in *Proc. 11th IEEE Int. Conf. Control Automat.*, Jun. 2014, pp. 1072–1077.

[19] D. Xu, J. Zhang, B. Zhou, and H. Yu, "Investigation of mode transition coordination for power-split hybrid vehicles using dynamic surface control," *Proc. Inst. Mech. Eng., K, J. Multi-Body Dyn.*, vol. 233, no. 3, pp. 696–713, Sep. 2019.

[20] J. Yao and W. Deng, "Active disturbance rejection adaptive control of uncertain nonlinear systems: Theory and application," *Nonlinear Dyn.*, vol. 89, no. 3, pp. 1611–1624, Aug. 2017.

[21] H. Pan, X. Jing, W. Sun, and H. Gao, "A bioinspired dynamics-based adaptive tracking control for nonlinear suspension systems," *IEEE Trans. Control Syst. Technol.*, vol. 26, no. 3, pp. 903–914, May 2018.

[22] J. Wang, T. Yan, Y. Bai, Z. Luo, X. Li, and B. Yang, "Assistance quality analysis and robust control of electric vehicle with differential drive assisted steering system," *IEEE Access*, vol. 8, pp. 136327–136339, 2020.

[23] H. Pan, W. Sun, H. Gao, and X. Jing, "Disturbance observer-based adaptive tracking control with actuator saturation and its application," *IEEE Trans. Autom. Sci. Eng.*, vol. 13, no. 2, pp. 868–875, Apr. 2016.

[24] N. Sun, D. Liang, Y. Wu, Y. Chen, Y. Qin, and Y. Fang, "Adaptive control for pneumatic artificial muscle systems with parametric uncertainties and unidirectional input constraints," *IEEE Trans. Ind. Informat.*, vol. 16, no. 2, pp. 969–979, Feb. 2020.

[25] H. Pan and W. Sun, "Nonlinear output feedback finite-time control for vehicle active suspension systems," *IEEE Trans. Ind. Informat.*, vol. 15, no. 4, pp. 2073–2082, Apr. 2019.

[26] T. Yang, N. Sun, H. Chen, and Y. Fang, "Observer-based nonlinear control for tower cranes suffering from uncertain friction and actuator constraints with experimental verification," *IEEE Trans. Ind. Electron.*, early access, May 12, 2020, doi: 10.1109/TIE.2020.2992972.

[27] R. Sanz, P. García, E. Fridman, and P. Albertos, "Robust predictive extended state observer for a class of nonlinear systems with time-varying input delay," *Int. J. Control*, vol. 93, no. 2, pp. 217–225, Feb. 2020.

[28] J. Yao and W. Deng, "Active disturbance rejection adaptive control of hydraulic servo systems," *IEEE Trans. Ind. Electron.*, vol. 64, no. 10, pp. 8023–8032, Oct. 2017.

[29] M. Pu, P. Liu, and A. Xiong, "Advanced fal function and three novel nonlinear extended state observers," *Control Decis.*, to be published, doi: 10.13195/j.kzyjc.2019.1652.

[30] B. Du, D. T. Qin, and Z. H. Duan, "Multi—Domain physical modeling and mode switching control simulation of HEV," *J. Syst. Simul.*, vol. 25, no. 7, pp. 1668–1674, Jul. 2013.

[31] D. H. Shi, "Research on hybrid dynamic modeling and optimal control of the energy management system for power split hybrid electric vehicle," Ph.D. dissertation, Dept. Automot. Eng., Jiangsu Univ., Zhenjiang, China, 2017.

[32] Z. G. Zhao, L. X. Jiang, M. N. Li, and M. Y. Wang, "Torque coordinated control during mode switching of a compound power-split hybrid system based on reference model," *Automot. Eng.*, vol. 40, no. 10, pp. 1132–1138, Oct. 2018.

[33] H. X. Li, "Mode switching coordinated control strategy of HEV based on robust control theory," M.S. thesis, Dept. Automot. Eng., Henan Univ. Sci. Technol, Luoyang, China, 2018.

[34] B. Du, X. F. Yin, and Y. Yang, "Robust control of mode transition for a single-motor full hybrid electric vehicle," *Adv. Mech. Eng.*, vol. 9, no. 9, pp. 1–16, Sep. 2017.

[35] B. X. Wen, W. D. Wang, C. L. Xiang, F. Ding, and Y. L. Qi, "Coordination control based on μ-synthesize for electro-mechanical transmission," *J. Mech. Eng*, vol. 53, no. 14, pp. 88–97, Aug. 2016.

[36] X. L. Tang, K. Yang, T. Liu, Y. C. Qin, D. J. Zhang, and Q. H. Ji, "Transient dynamic response analysis of engine start for a hybrid electric vehicle," presented at the 3rd Conf. Vehicle Control Int. (CVCI), Hefei, China, Sep. 2020.

[37] L. Chen, G. Xi, and J. Sun, "Torque coordination control during mode transition for a series–parallel hybrid electric vehicle," *IEEE Trans. Veh. Technol.*, vol. 61, no. 7, pp. 2936–2949, Sep. 2012.

[38] Z. S. Yu, *Automotive Theory*, 3rd ed. Beijing, China: China Mach. Press, 2000, pp. 1–279.

LONG CHEN was born in Jinjiang, China, in 1958. He received the B.S. and Ph.D. degrees from Jiangsu University, in 1982 and 2006, respectively.

He is currently a Professor and a Ph.D. Supervisor with the Automotive Engineering Research Institute, Jiangsu University, Jiangsu, China. He is leading three research projects funded by the National Natural Science Foundation of China and more than ten other national and provincial research projects in China. He has published more than 100 academic articles. His research interests include road traffic safety and management, vehicle active safety technology, and vehicle dynamic simulation and control.

Dr. Chen was a recipient of the Chinese Mechanical Industry Young Scientist Award for Excellence, the Young and Middle-aged Expert Award for Outstanding Contribution to Jiangsu Province, and the Jiangsu Provincial Science and Technology Progress Award.

JIAJIA WANG was born in Xinyang, China, in 1992. She received the M.S. degree in vehicle engineering from Jiangsu University, China, in 2017, where she is currently pursuing the Ph.D. degree.

Her research interests include vehicle dynamic performance simulation and control and hybrid electric vehicles.

YINGFENG CAI (Member, IEEE) was born in Jiangsu, China, in 1985. She received the B.S. degree in measurement and control technology and instruments, the M.S. degree in precision instrument and mechanics, and the Ph.D. degree from Southeast University, Jiangsu, China, in 2006, 2009, and 2013, respectively.

She has published more than 75 academic articles, which covers intelligent vehicle information perception and control technology, automatic driving technology, and so on.

Dr. Cai was the Co-Chairman of the Committee of Young Scientists of the IEEE Robotics and Automation Society and a reviewer for several domestic and international academic journals.

DEHUA SHI received the B.S. and Ph.D. degrees in automotive engineering from Jiangsu University, in 2011 and 2017, respectively. In 2017, he joined the Automotive Engineering Research Institute, Jiangsu University. His research interests include energy management of hybrid electric vehicles, and simulation and control of vehicle system dynamics.

RUOCHEN WANG was born in Xinyang, China, in 1977. He received the Ph.D. degree from Jiangsu University, in 2006. He is currently a Professor and a Ph.D. Supervisor with the Automotive Engineering Research Institute, Jiangsu University, Jiangsu, China. His research interests include intelligent vehicle systems, new energy vehicles, and vehicle dynamic simulation and control.